MOLECULAR PHYSICS, 1990, VOL. 69, NO. 2, 241–263

Combined shear and elongational flow by non-equilibrium molecular dynamics

by M. W. EVANS† and D. M. HEYES
Department of Chemistry, Royal Holloway and Bedford New College, University of London, Egham, Surrey TW20 0EX, England

(*Received 26 June 1989; accepted 13 October 1989*)

We continue our development of group theory statistical mechanics applied to non-newtonian shear and elongational flow. We discuss some new aspects of shear flow discovered by non-equilibrium molecular dynamics, NEMD. We investigate the origins of time reversal asymmetry in newly discovered cross-correlation functions. Using the profile unbiased thermostat, PUT, shear flow algorithm we discover that the strong phase is stable in 3D, for typical system sizes considered by molecular dynamics. In addition, for the *first* time we apply NEMD, to simultaneous shear and elongational non-newtonian flow. New equations of motion are constructed to enforce the elongational flow. We apply transient flows to a model Lennard-Jones liquid and monitor the thermodynamics and mechanical response, directly, and from transient time correlation functions. The value of the shear viscosity can be increased or lowered by the presence of simultaneous shear and elongational flow, in which the main velocity flow directions are perpendicular or parallel, respectively. A combination of shear and elongational flow can produce a heat flux, the thermal equivalent of the Weissenberg effect.

1. Introduction

We have recently demonstrated [1–2] that a shear rate, $\partial v_X/\partial Y$, induces *newly discovered* time asymmetric cross correlation functions of velocity in the laboratory frame XYZ which are irreversible and asymmetric to time displacement (i.e. breaking the Onsager–Casimir symmetry of equilibrium correlation functions [3–7]), i.e.

$$\langle v_X(0)v_Y(t)\rangle \neq \langle v_X(t)v_Y(0)\rangle. \tag{1}$$

These results break the Onsager–Casimir symmetry and violate Onsager's reciprocal relation at arbitrarily small applied field. This discovery therefore applies in 'linear' or 'non-linear' response regimes. The theory was described that predicts those time-correlation functions existing in (symmetry breaking) simple planar shear flow, which are trivially zero in the absence of shear flow for symmetry reasons. The cross correlation functions of this type are predicted by the third principle of group

† Visiting Academic at IBM, Data Systems Division, Neighbourhood Road, Kingston, New York 12401, U.S.A. Also Honorary Research Fellow, Department of Physics, University of Lancaster, Lancaster LA1 4YB, England.

theoretical statistical mechanics, GTSM. Their observation using an assumed (linear) profile thermostat, SSLOD, NEMD [1] and subsequently by a profile unbiased thermostat, PUT in 2D and 3D [8] vindicated the generality of the predictions of the axioms of GTSM.

The result (1) is given by the third principle of GTSM, [1], which states that an applied external field of given symmetry *may* induce new thermodynamic averages in an ensemble at field-applied steady state. These averages take the symmetry of the field itself. The symmetry arguments for the appearance of the shear induced cross-correlation functions depend on group theory in the laboratory frame XYZ defined by the three dimensional rotation–reflection group, $R_h(3)$, with irreducible representations denoted by the D symbols, $D_g^{(0)}, \ldots, D_g^{(n)}$ and $D_u^{(1)}, \ldots, D_u^{(n)}$, respectively; where the subscript, **g** (or gerade) denotes even to parity reversal symmetry and **u** (or ungerade) denotes odd to parity reversal symmetry (i.e. $(\mathbf{q}, \mathbf{p}) \rightarrow (-\mathbf{q}, -\mathbf{p})$). The superscipts refer to the order of the spherical harmonics. The D symmetry of the strain rate was shown to be,

$$\Gamma(\mathbf{v})\Gamma(\mathbf{r}^{-1}) = D_u^{(1)} D_u^{(1)} = D_g^{(0)} + D_g^{(1)} + D_g^{(2)}. \tag{2}$$

The irreducible representation, $D_g^{(0)} + D_g^{(1)} + D_g^{(2)}$, of the strain rate tensor reflects the fact that it has an antisymmetric component of vorticity, of symmetry, $D_g^{(1)}$, and a symmetric component of symmetry, $D_g^{(0)} + D_g^{(2)}$. The $D_g^{(1)}$ component is a vector product and the $D_g^{(2)}$ component is a symmetric tensor product. The response to the pure strain rate tensor has symmetry $D_g^{(2)}$. Therefore we have, for shear flow specifically,

$$\begin{pmatrix} 0 & 0 & 0 \\ 0 & 0 & 0 \\ 0 & 0 & 0 \end{pmatrix}(D_g^{(0)}) + \begin{pmatrix} 0 & \dot\gamma/2 & 0 \\ -\dot\gamma/2 & 0 & 0 \\ 0 & 0 & 0 \end{pmatrix}(D_g^{(1)}) + \begin{pmatrix} 0 & \dot\gamma/2 & 0 \\ \dot\gamma/2 & 0 & 0 \\ 0 & 0 & 0 \end{pmatrix}(D_g^{(2)}),$$

where $\dot\gamma$ is a constant shear rate. GTSM tells us that the tensor symmetry of all time correlation functions of the type, $\langle \mathbf{A}(0)\mathbf{A}^{\mathrm{T}}(t)\rangle$, where **A** is a polar or axial vector representing a molecular property, is also $D_g^{(0)} + D_g^{(1)} + D_g^{(2)}$. The term, $D_g^{(0)}$, represents the trace or the diagonal sum of the cross correlation tensor, for example for velocity, **v**,

$$C_v(t) = \langle \mathbf{v}(0)\mathbf{v}^{\mathrm{T}}(t)\rangle, \tag{3}$$

which has the same D symmetry as the strain rate tensor. Here $\langle \ldots \rangle$ denotes an average over time origins, where, for $t > 0$ at least, the system is not at equilibrium. When the latter has planar couette shear symmetry, the induced ccf (3) is traceless [1, 2]. The vector and tensor parts of the symmetry signature represent, by principle (3), the time antisymmetric and time symmetric cross correlation functions [1]

$$D_g^{(1)}: \langle v_X(0)v_Y(t)\rangle = -\langle v_Y(0)v_X(t)\rangle, \tag{4}$$

and

$$D_g^{(2)}: \langle v_X(0)v_Y(t)\rangle = \langle v_Y(0)v_X(t)\rangle, \tag{5}$$

respectively. Although they separately obey the Onsager–Casimir symmetry, i.e. are either negative or positive to time reversal, and $\partial v_X/\partial Y$ field in general produces a weighted sum of (4) and (5) to give the asymmetric result (1). This was noted in the

previous study in this
Onsager's reciprocal r
an imposed strain rat
atory XYZ frame of
pressure tensor compo

and

We demonstrate, ther
sical description of rh

If the shear strain
$\langle v_X(t)v_Y(0)\rangle$, $\langle P_{\alpha X}(t)P_{\alpha$
XYZ frame and $P_{\alpha\beta}$
$\langle P_{XZ}(0)P_{YZ}(t)\rangle$, $\langle P_{XY}$
also these ccfs with ti
tions under nonequili

In this study we
$\partial v_X/\partial X$, $\partial v_y/\partial Y$ and
considered. Within th
10^3 molecules, a stea
long time to obtain r
gational flow, this wa
flows (lasting for 3–4
space [9, 10]. A serie
averaging. At the sm
before the end of th
non-newtonian stead

The symmetry a
response regime and
they may be applie
alization [11–13] o
response to arbitrary

where $\langle \ldots \rangle$ represen
Here $B(t)$ is an arbitr

where H is the ham
$B(s)$ evolves from $B(0$

The response to
and thereby brough
predicts that elonga

previous study in this series [2]. This is the *first* observation of a counter example to Onsager's reciprocal relation, applying at all strain rates. Thus according to GTSM, an imposed strain rate, $\partial v_X/\partial Y$ in couette flow induces the existence in the laboratory XYZ frame of the time correlation functions (4) and (5). Similarly for the pressure tensor components we have,

$$\langle P_{XZ}(0)P_{YZ}(t)\rangle = -\langle P_{YZ}(0)P_{XZ}(t)\rangle, \tag{6}$$

and

$$\langle P_{XZ}(0)P_{YZ}(t)\rangle = \langle P_{YZ}(0)P_{XZ}(t)\rangle. \tag{7}$$

We demonstrate, therefore, a new link between microscopic dynamics and the classical description of rheology involving pure strain rate and vorticity terms.

If the shear strain rate is $\dot{\gamma} = \partial v_X/\partial Y$, the new cross-correlations are of the type $\langle v_X(t)v_Y(0)\rangle$, $\langle P_{\alpha X}(t)P_{\alpha Y}(0)\rangle$ and $\langle P_{\alpha\alpha}(t)P_{XY}(0)\rangle$, where $\mathbf{v}$ is the atomic velocity in the XYZ frame and $P_{\alpha\beta}$ is the $\alpha\beta$ component of the pressure tensor [1, 2]. That is, $\langle P_{XZ}(0)P_{YZ}(t)\rangle$, $\langle P_{XY}(0)P_{XX}(t)\rangle$, $\langle P_{XY}(0)P_{YY}(t)\rangle$ and $\langle P_{XY}(0)P_{ZZ}(t)\rangle$. This includes also these ccfs with time arguments reversed, which as noted can be different functions under nonequilibrium conditions.

In this study we also apply GTSM for the first time to elongational flow, $\partial v_X/\partial X$, $\partial v_y/\partial Y$ and $\partial v_Z/\partial Z$. Also simultaneous elongational and shear flow are considered. Within the usual restriction of the simulation cells containing $N \sim 10^2$–10^3 molecules, a steady state elongational flow cannot be achieved for a sufficiently long time to obtain reasonable statistical averages. In previous simulations of elongational flow, this was overcome by implementing a series of transient elongational flows (lasting for 3–4 ps for Ar) starting from different points in equilibrium phase space [9, 10]. A series of short-lived steady states was achieved for the purpose of averaging. At the small strain rates considered here a steady state can be achieved before the end of the transient, making this approach suitable for investigating non-newtonian steady states. This approach is applied here.

The symmetry arguments of GTSM are valid outside the customary linear response regime and for the transient phenomena implemented here. In particular, they may be applied to both sides of the important *new* Evans–Morriss generalization [11–13] of the fluctuation–dissipation theorem extended from linear response to arbitrary field strength, F_e

$$\langle B(t)\rangle = \langle B(0)\rangle - \frac{F_e}{k_B T}\int_0^t \langle B(s)J(0)\rangle\, ds, \tag{8}$$

where $\langle\ldots\rangle$ represents an average over an equilibrium ensemble over initial states. Here $B(t)$ is an arbitrary phase variable and J is the dissipative flux defined by,

$$\frac{dH}{dt} = -JF_e, \tag{9}$$

where H is the hamiltonian. $B(0)$ and $J(0)$ are evaluated in the field-free ensemble. $B(s)$ evolves from $B(0)$ with field-on dynamics initiated at $s = 0$.

The response to a suddenly applied field is now related to a correlation function, and thereby brought within the framework of GTSM. Principle (3) of GTSM [2] predicts that elongational flow field should induce new transient time correlation

functions of the form,

$$\langle A_i(0)A_i(t)\rangle, \quad i = X, Y, Z, \tag{10}$$

whose D symmetry is $D_g^{(0)}$. Examples of these correlation functions are, $\langle v_X(0)v_X(t)\rangle$, $\langle v_Y(0)v_Y(t)\rangle$, $\langle v_Z(0)v_Z(t)\rangle$, $\langle P_{XX}(0)P_{XX}(t)\rangle$, $\langle P_{YY}(0)P_{YY}(t)\rangle$ and $\langle P_{ZZ}(0)P_{ZZ}(t)\rangle$, where $\mathbf{P}$ is the pressure tensor. Here we are interested in the transient time correlation functions. Therefore the quantity at time $t = 0$ is taken from the equilibrium ensemble, whereas the quantity at time $t > 0$ is taken from the non-equilibrium state.

Another new feature of this work is the simultaneous application of shear and elongational strain rates, which frequently occurs in the complex strain rate distribution found in processing flows, [14]. If the elongational strain is accompanied by shear strain we expect correlation functions of the type (2). A combination of shear and elongational strains will give rise to cross transient time correlation functions of both the off-diagonal type (1) and the diagonal type (10). Using (8) we also note that the response functions directly observed also share these symmetry properties.

The transient ccfs of type (10) have symmetry $D_g^{(0)}$ and there clearly cannot be asymmetric in index reversal as in (1). (It is impossible to have $v_X(0)v_X(t)\rangle = -\langle v_X(t)v_X(0)\rangle$.) Therefore the ccf induced by 'stretching' or elongational flow are of the diagonal type with no vorticity and no off-diagonal type deformation. The time dependence of $\langle A_i(0)A_i(t)\rangle$, $i = X, Y, Z$, is determined by the elongational strain. They also exist at shear- and elongation-free equilibrium because they have the scalar signature $D_g^{(0)}$. The latter signature refers to the trace, and individual elements of the trace may have a different time dependence under elongational shear strain or stress. If shear stress is added to elongational stress then the *time-dependence* of these diagonal elements might be changed from that caused by elongational stress alone.

In summary, shear stress induces off-diagonal ccfs which may be index asymmetric. In contrast, elongational stress induces diagonal elements which cannot be index (time) asymmetric.

2. Simulation details

In this section we describe methods for incorporating planar shear and elongational flow in the classical equations of motion of molecular dynamics.

The MD simulations followed particles of mass, m, interacting via the Lennard-Jones, LJ potential [9],

$$\phi(r) = 4\varepsilon((\sigma/r)^{12} - (\sigma/r)^6). \tag{11}$$

The basic technique is that used in a previous MD study [1]. The MD simulations were performed on a cubic unit cell of volume V containing $N = 256$ and $N = 500$ for the transient flows and $N = 500$ for the steady state shear flows. The interactions were truncated at $2{\cdot}5\sigma$. We use LJ reduced units throughout, i.e. $k_B T/\varepsilon \to T$, and number density, $\rho = N\sigma^3/V$. Time is in $\sigma(m/\varepsilon)^{1/2}$, strain rate is in $(\varepsilon/m)^{1/2}/\sigma$, viscosity is in $(m\varepsilon)^{1/2}/\sigma^2$ and stress is in $\varepsilon\sigma^{-3}$. The temperature was fixed by velocity rescaling of the peculiar velocities [15, 16]. The time step was 0·015. The state point mainly considered was a near triple point state, at $\rho = 0{\cdot}8442$ and $T = 0{\cdot}722$. In the

sheared case, $\dot{\gamma} = 1{\cdot}0$,
stress and thermodyr
$(\phi(r))$ dependent term

We used the SLL
thermal velocity is de

where the α compor
peculiar velocity is $\tilde{v}_\alpha$
flow velocity). We r
Verlet algorithm usi
lation functions were
with appropriate sy
reduce the noise at lo
We calculated the

where

P_{XY}

where r_{xij} is the x co
Some simulations
[19, 20]. In SLLOD
procedure. Any devi
temperature and dul
taneous shear velocit
than SLLOD at high
fluctuations about th
is more realistically
differs from that of

sheared case, $\dot{\gamma} = 1{\cdot}0$, produces $\eta = 2{\cdot}1$, about 30 per cent shear thinning [17]. The stress and thermodynamic properties are governed mainly by the configurational ($\phi(r)$) dependent terms.

2.1. *Shear flow*

We used the SLLOD algorithm in most of the calculations [18]. The peculiar or thermal velocity is denoted by $\tilde{v}$. For molecular position, $\mathbf{R}$,

$$\dot{R}_X = v_X = \tilde{v}_X + \dot{\gamma} R_Y, \tag{12}$$

$$\dot{R}_Y = v_Y = \tilde{v}_Y, \tag{13}$$

$$\dot{R}_Z = v_Z = \tilde{v}_Z, \tag{14}$$

$$\frac{d\tilde{v}_X}{dt} = F_X/m - \dot{\gamma}\tilde{v}_Y, \tag{15}$$

$$\frac{d\tilde{v}_Y}{dt} = F_Y/m, \tag{16}$$

$$\frac{d\tilde{v}_Z}{dt} = F_Z/m, \tag{17}$$

where the α component of the force on a particle is F_α, the velocity is v_α, the peculiar velocity is $\tilde{v}_\alpha$ (i.e. that component of the velocity in excess of the streaming flow velocity). We maintain constant kinetic energy ('temperature') within the Verlet algorithm using *velocity* rescaling applied to $\tilde{v}_\alpha$. The transient time correlation functions were determined using the method of Evans and Morris [11–13] with appropriate symmetry mappings of the equilibrium phase state points to reduce the noise at long time.

We calculated the shear viscosity, η, from,

$$\eta = -P_{XY}/\dot{\gamma}, \tag{18}$$

where

$$P_{XY} = \frac{1}{V}\left(\sum_{i=1}^{N} m_i \tilde{v}_{xi}\tilde{v}_{yi} - \sum_{i=1}^{N-1}\sum_{j>i}^{N}(r_{xij}r_{yij}/r_{ij})\frac{d\phi(r_{ij})}{dr}\right), \tag{19}$$

where r_{xij} is the x component of $\mathbf{r}_{ij}$ and $V = (N/\rho)$, the volume of the MD cell.

Some simulations were also carried out at steady state using the PUT algorithm [19, 20]. In SLLOD a linear velocity profile $v_X(Y)$ is assumed in the thermostatting procedure. Any deviations from this will be taken as an extra contribution to the temperature and duly suppressed. In PUT no assumption is made about the instantaneous shear velocity distribution within the MD cell. It is therefore more realistic than SLLOD at high shear rates because it naturally incorporates the local velocity fluctuations about the mean (from the shear rate). Therefore the onset of turbulence is more realistically modelled. Our implementation of the PUT equations of motion differs from that of Evans and Morriss, in determining a local temperature for each

particle from its local drift velocity. The instantaneous average drift velocity around each particle is obtained by summing the velocities within an enclosed sphere. A spherical truncation radius of value, $r_p = 1{\cdot}5$ or $2{\cdot}0\sigma$ was typically used. (Properties were only moderately sensitive to values of r_p in this range.)

2.2. *Elongational flow*

The equations for elongational flow are similar to those for shear flow.

$$\dot{R}_X = v_X = \tilde{v}_X + \dot{\gamma}_X R_X, \tag{20}$$

$$\dot{R}_Y = v_Y = \tilde{v}_Y + \dot{\gamma}_Y R_Y, \tag{21}$$

$$\dot{R}_Z = v_Z = \tilde{v}_Z + \dot{\gamma}_Z R_Z, \tag{22}$$

$$\frac{d\tilde{v}_X}{dt} = F_X/m - \dot{\gamma}_X \tilde{v}_X, \tag{23}$$

$$\frac{d\tilde{v}_Y}{dt} = F_Y/m - \dot{\gamma}_Y \tilde{v}_Y, \tag{24}$$

and

$$\frac{d\tilde{v}_Z}{dt} = F_Z/m - \dot{\gamma}_Z \tilde{v}_Z. \tag{25}$$

Again thermostatting was performed using velocity rescaling. For convenience, we define $\dot{\gamma}_X = \dot{\gamma}_T \delta_X$, $\dot{\gamma}_Y = \dot{\gamma}_T \delta_Y$ and $\dot{\gamma}_Z = \dot{\gamma}_T \delta_Z$. Elongational flow has $\delta_X = 1$, $\delta_Y = -1/2$ and $\delta_Z = -1/2$ or any permutation of this sequence. We consider here two elongational strain geometries.

(i) $\delta_X = 1, \delta_Y = -1/2$ and $\delta_Z = -1/2$,
(ii) $\delta_X = -1/2, \delta_Y = 1$ and $\delta_Z = -1/2$.

We calculated the tensile viscosity, η_T, from,

$$\eta_T = \sum_\alpha \delta_\alpha P_{\alpha\alpha}/\dot{\gamma}_T, \tag{26}$$

where

$$P_{\alpha\alpha} = \frac{1}{V}\left(\sum_{i=1}^{N} m_i \tilde{v}_{\alpha i}\tilde{v}_{\alpha i} - \sum_{i=1}^{N-1}\sum_{j>1}^{N} (r_{\alpha ij} r_{\alpha ij}/r_{ij}) \frac{d\phi(r_{ij})}{dr}\right). \tag{27}$$

As the fluid MD cell is periodically repeated in all three dimensions, the elongational flow should only be susceptible to similar finite N artefacts as for shear flow. There is a constraint that must be satisfied in elongational flow, which is absent in the pure shear flow simulations. There is upper limit on $\dot{\gamma}_T$, determined so that none of the cell dimensions, sidelength L, should be less than twice the pair potential truncation distance (i.e. 5σ) at any time during the elongation transient. (The maximum distortion occurs at the end of the transient, as $L(t)/L(0) = \exp(\dot{\gamma}_\alpha t)$.) Despite there being this upper bound on $\dot{\gamma}_T$ the range of allowable $\dot{\gamma}_T$ was sufficient to capture newtonian and non-newtonian phenomena broadly comparable to those

of shear flow up to $\dot{\gamma}$
(26) in the plateau re
material structurally
occurs. The value of
involved.

Computations we
University of London

In steady state sh

$\langle \tilde{v}_Z(0)\tilde{v}_X(t)\rangle$,
$(V/k_B T)\langle P_{XZ}(0)$
$(V/k_B T)\langle P_{XZ}(0)$
$(V/k_B$

GTSM predicts
shear flow: $\langle \tilde{v}_Y(0)\tilde{v}_X($
$(V/k_B T)\langle P_{XY}(0)P_{YY}(t$
zero functions and a
the above ccfs. Not
velocities. The existe
is chosen.

The strain rate t
symmetric traceless
ponent associated w
torted fluid structur
Introduction, GTSI
function induced at
to time or index rev
strain rate compone
the effect of vorticit
reversal, as will be s
observation of an a
simulation, and the
terms of the ccf.

The general fea
[1]. However, there
flow which we discu
the 3D simulations
state.

The $\langle P_{XZ}(0)P_Y$
$T = 0{\cdot}722$, $\dot{\gamma} = 20{\cdot}0$
finite negative val
$\nu \sim \dot{\gamma}/2$. This oscill
in which the mole
triangular lattice w

of shear flow up to $\dot{\gamma} \sim 0{\cdot}5$. The elongational viscosities are obtained by applying (26) in the plateau region of the response, should one be manifest. At high $\dot{\gamma}_T$ the material structurally degrades before a plateau in either shear or elongational stress occurs. The value of this critical $\dot{\gamma}_T$ depends on ρ, T and $\dot{\gamma}$ if shear flow is also involved.

Computations were carried out in single precision on a CRAY-XMP at the University of London Computer Centre.

3. Results and discussion

3.1. *Shear flow*

In steady state shear we evaluated the cross correlation functions,

$$\langle \tilde{v}_Z(0)\tilde{v}_X(t)\rangle,\quad \langle \tilde{v}_Y(0)\tilde{v}_X(t)\rangle,\quad \langle \tilde{v}_Y(0)\tilde{v}_X(t)\rangle,\quad (V/k_B\,T)\langle P_{XY}(0)P_{XY}(t)\rangle,$$
$$(V/k_B\,T)\langle P_{XZ}(0)P_{XZ}(t)\rangle,\quad (V/k_B\,T)\langle P_{YZ}(0)P_{YZ}(t)\rangle,\quad (V/k_B\,T)\langle P_{XZ}(0)P_{YZ}(t)\rangle,$$
$$(V/k_B\,T)\langle P_{XZ}(0)P_{XY}(t)\rangle,\quad (V/k_B\,T)\langle P_{XY}(0)P_{YZ}(t)\rangle,\quad (V/k_B\,T)\langle P_{XY}(0)P_{XX}(t)\rangle,$$
$$(V/k_B\,T)\langle P_{XY}(0)P_{YY}(t)\rangle \quad \text{and} \quad (V/k_B\,T)\langle P_{XY}(0)P_{ZZ}(t)\rangle.$$

GTSM predicts that the following correlation functions could exist in dv_X/dY shear flow: $\langle \tilde{v}_Y(0)\tilde{v}_X(t)\rangle$, $\langle \tilde{v}_X(0)\tilde{v}_Y(t)\rangle$, $(V/k_B\,T)\langle P_{XZ}(0)P_{YZ}(t)\rangle$, $(V/k_B\,T)\langle P_{XY}(0)P_{XX}(t)\rangle$, $(V/k_B\,T)\langle P_{XY}(0)P_{YY}(t)\rangle$ and $(V/k_B\,T)\langle P_{XY}(0)P_{ZZ}(t)\rangle$. We observed all of these as non-zero functions and also the different ccfs formed by reversing the time arguments in the above ccfs. Note that the velocity ccfs can be defined in terms of $\tilde{\mathbf{v}}$ or $\mathbf{v}$ velocities. The existence of these functions is independent of which of these velocities is chosen.

The strain rate tensor in planar couette flow of the type dv_X/dY consists of a symmetric traceless or 'pure strain rate' component and an antisymmetric component associated with vorticity. The latter causes a rotation of the primarily distorted fluid structure away from the $\pi/4$ and $3\pi/4$ directions. As mentioned in the Introduction, GTSM, reveals that there are two types of time-cross correlation function induced at the microscopic level by $\partial v_X/\partial Y$ flow [1, 2, 8]. One is symmetric to time or index reversal (i.e. $(\mathbf{q}, \mathbf{p}) \rightarrow (\mathbf{q}, -\mathbf{p})$) and represents the effect of the pure strain rate component. The other is antisymmetric to index reversal and represents the effect of vorticity. The sum of both influences is generally asymmetric to a time reversal, as will be shown by SLLOD and PUT NEMD simulations. This is the *first* observation of an antisymmetric time cross-correlation function, ccf, by computer simulation, and the *first* successful resolution of pure strain rate and vorticity in terms of the ccf.

The general features of the ccfs have been discussed in a previous publication [1]. However, there are a number of new points in the case of *steady-state* couette flow which we discuss first before moving on to the transient flows. We first consider the 3D simulations performed on a high density state point near the LJ triple point state.

The $\langle P_{XZ}(0)P_{YZ}(t)\rangle$ and $\langle P_{XZ}(t)P_{YZ}(0)\rangle$ for the PUT 3D LJ $\rho = 0{\cdot}8442$, $T = 0{\cdot}722$, $\dot{\gamma} = 20{\cdot}0$ and $N = 500$ state are shown in figure 1. They both start from a finite negative value and then decay in an oscillatory manner with frequency $\nu \sim \dot{\gamma}/2$. This oscillatory structure we attribute to the formation of a 'string' phase in which the molecules travel along the streamlines in lines packed together in a triangular lattice when viewed in cross-section (see figure 2). The PUT algorithm

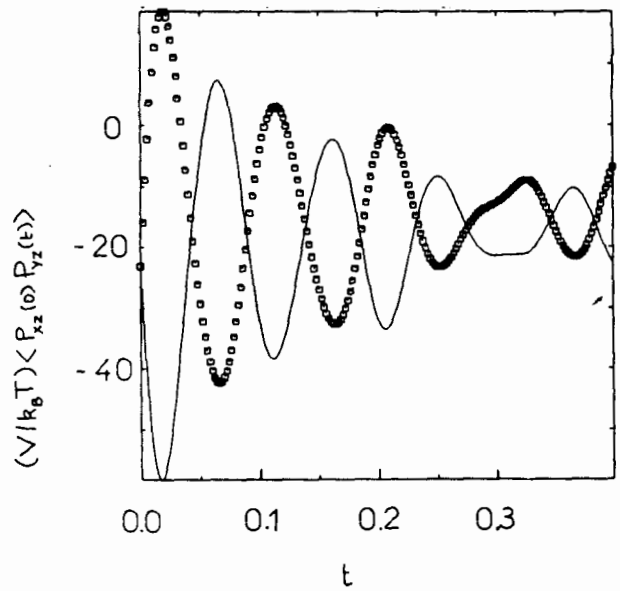

Figure 1. The time cross-correlation function $(V/k_BT)\langle P_{XZ}(0)P_{YZ}(t)\rangle$, solid line and $(V/k_BT)\langle P_{YZ}(0)P_{XZ}(t)\rangle$, squares using the PUT algorithm ($r_p = 2\sigma$) at the 3D LJ $N = 500$ state $\rho = 0{\cdot}8442$, $T = 0{\cdot}722$ and $\dot{\gamma} = 20$.

induces a string phase in 3D for these finite periodic systems in contrast to the case for 2D fluids [19]. 2D PUT simulations using the present method showed no string phase at the same state point as (and in agreement with) Evans and Morriss [19]. The lack of a string phase in 2D by both implementations of a profile unassumed thermostat makes the difference in behaviour in 3D more significant. The string phase in figure 2(*a*) is in the transition region between an amorphous and ordered phase ($\dot{\gamma} \sim 2$–3) [17]. This is why it shows some remnants of the amorphous fluid phase in comparison with the highly ordered $\dot{\gamma} = 20$ state of figure 2(*b*). The simulations were repeated starting from a truly fluid state to verify that the string phase produced by the PUT algorithm in 3D is well-defined and not a product of hysteresis. Adjacent molecules in neighbouring strings are separated by a distance $\sim\sigma$. The relative velocity between these molecules in the streaming direction is $\sim\sigma\dot{\gamma}$. Hence the frequency of registry of molecules is $\sim\dot{\gamma}$. Irrespective of the wider debate concerning the existence of the string phase in monoatomic fluids, figure 1 is noteworthy because the time-reversed function, $\langle P_{YZ}(0)P_{XZ}(t)\rangle$, is significantly different, being neither symmetric nor antisymmetric to $\langle P_{XZ}(0)P_{YZ}(t)\rangle$. This can be traced to the contribution and dominance of the vorticity component of the flow, which unlike the pure strain component of the strain rate tensor, has negative symmetry to time reversal. (Calculations with $N = 108$ produced the same time-reversal asymmetry, revealing that this effect is independent of N).

Following on from previous gas phase simulations of shear flow [21] we investigate the ccfs at the low density LJ state, $\rho = 0{\cdot}1$ and $T = 2{\cdot}5$. At low density there is no string phase so that many of the distinctive features associated with shear thinking at liquid density are lost. The same ccfs appear in the gas phase, again manifesting time irreversibility. (The SLLOD ccfs are more pronounced but basically have the same form.) The time correlation function, $\langle \tilde{v}_Y(0)\tilde{v}_X(t)\rangle$, which in the absence of

Figure 2. Scattergra
with $N = 500$
of the LJ parti
long-range stru
SLLOD, and (*b*

shear flow is zero a
the SLLOD algorit

Table 1 shows t
$\langle \tilde{v}_X(0)\tilde{v}_Y(0)\rangle$ is ap
($\eta = 3{\cdot}5 \pm 0{\cdot}1$ for $\dot{\gamma}$
tant macroscopic p
non-newtonian rhe

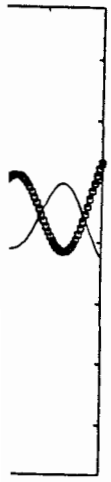

$0)P_{YZ}(t)\rangle$, solid line and
$(r_p = 2\sigma)$ at the 3D LJ

in contrast to the case
ethod showed no string
vans and Morriss [19].
of a profile unassumed
significant. The string
morphous and ordered
of the amorphous fluid
figure 2 (*b*). The simula-
y that the string phase
ot a product of hyster-
ted by a distance $\sim\sigma$.
ning direction is $\sim\sigma\dot{\gamma}$.
ive of the wider debate
fluids, figure 1 is note-
significantly different,
. This can be traced to
nt of the flow, which
negative symmetry to
ie time-reversal asym-

r flow [21] we investi-
At low density there is
ated with shear think-
phase, again manifest-
ed but basically have
nich in the absence of

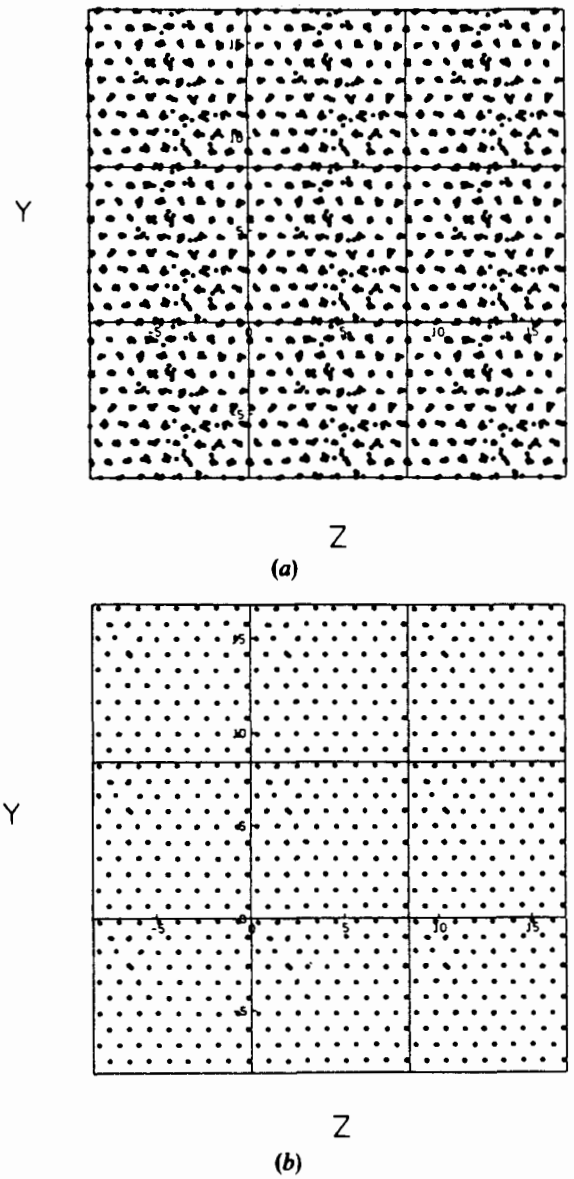

Figure 2. Scattergrams for 3D sheared LJ fluids at the 3D LJ state $\rho = 0{\cdot}8442$, $T = 0{\cdot}722$ with $N = 500$ using the PUT and SLLOD algorithms. The projections of the centres of the LJ particles onto the YZ plane are shown. To facilitate the observation of any long-range structure, the real MD cell and surrounding 8 images are given. (*a*) $\dot{\gamma} = 3{\cdot}0$, SLLOD, and (*b*) $\dot{\gamma} = 20$, PUT, $r_p = 2{\cdot}0$.

shear flow is zero at all times, t, is shown in figure 3, for the gas phase state using the SLLOD algorithm.

Table 1 shows that the amplitude of these new cross correlation functions, ccfs, $\langle \tilde{v}_X(0)\tilde{v}_Y(0)\rangle$ is approximately proportional to the extent of shear thinning ($\eta = 3{\cdot}5 \pm 0{\cdot}1$ for $\dot{\gamma} = 0$). The ccfs are therefore a microscopic probe of this important macroscopic property. This may lead ultimately to spectroscopic probes of non-newtonian rheology.

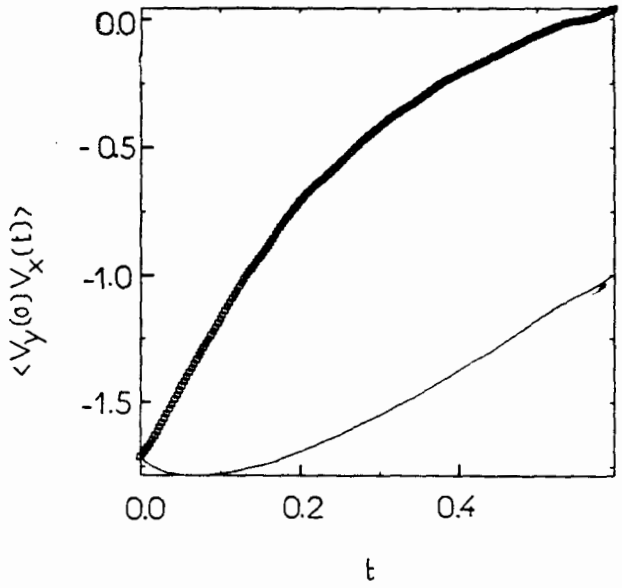

Figure 3. The peculiar velocity time correlation functions $\langle \tilde{v}_Y(0)\tilde{v}_X(t)\rangle$ (solid line) and $\langle \tilde{v}_X(0)\tilde{v}_Y(t)\rangle$ (squares) using SLLOD at the 3D LJ $N = 500$ state, $\rho = 0{\cdot}1$, $T = 2{\cdot}5$ and $\dot{\gamma} = 5$.

We now consider the transient response of simple liquids to shear flow suddenly applied at time $t = 0$, averaged over several thousand distinct starting phase points. They were performed with an assumed profile thermostat. The phase space mappings devised by Morriss and Evans were used [11]. If $\Gamma_1 = (x, y, z, p_x, p_y, p_z)$, the co-ordinates and momenta of an arbitrarily chosen particle, then three other starting phase points can be generated from this,

$$\Gamma_2 = (-x, -y, z, p_x, p_y, p_z),$$

$$\Gamma_3 = (-x, y, z, -p_x, p_y, p_z),$$

$$\Gamma_4 = (-x, y, z, p_x, -p_y, p_z).$$

This operation is applied to all molecules in the cell. Each of these operations gives a different response when subjected to a shear strain rate, $\partial v_X/\partial Y$.

Table 1. Ensemble averages for steady state shear PUT simulations at $\rho = 0{\cdot}8442$, $T = 0{\cdot}722$ using $N = 500$.

$\dot{\gamma}$	0·25	0·50	1·0
$\langle \tilde{v}_X(0)\tilde{v}_Y(0)\rangle$	−0·017	−0·038	−0·078
$\langle P_{YZ}(0)P_{XZ}(0)\rangle$	−2·4	−4·5	−6·4
$\langle P_{XX}(0)P_{XY}(0)\rangle$	−255	−737	−2449
$\langle P_{YY}(0)P_{XY}(0)\rangle$	−269	−788	−2618
$\langle P_{ZZ}(0)P_{XY}(0)\rangle$	−248	−645	−1886
η	2·71	2·44	2·11
$\langle P_{XX}\rangle$	0·44	0·73	1·40
$\langle P_{YY}\rangle$	0·47	0·78	1·50
$\langle P_{ZZ}\rangle$	0·44	0·65	1·09

$P_{x,y}(t)$

Figure 4. The stress r
jected to shear
and (c) $\dot{\gamma} = 1{\cdot}0$, ϵ

The transient resp
are given in figure 4.
2·46 and 2·13 ± 0·03
The viscosities are s
steady state SLLOD
(8) and the same m
example of the P_{XY} t
tensor component, P
6. The P_{XX} exhibits
reflecting the structu
Newtonian state. So
viscosity. The overs
comparable to that
not necessarily acco
the two lower shear

We now conside
point state. The pha
pressure component

Other permutations
Making use of t
starting points in pl

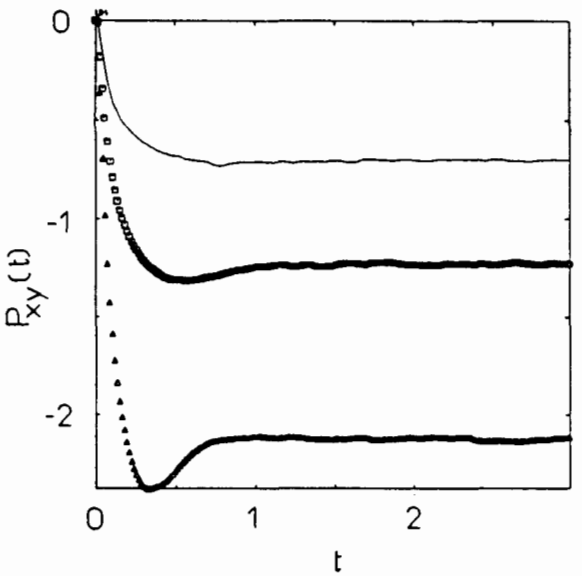

Figure 4. The stress responses, $P_{XY}(t)$, of $\rho = 0{\cdot}8442$ and $T = 0{\cdot}722$, $N = 256$ liquids subjected to shear strain rates applied at time $t = 0$: (*a*) $\dot{\gamma} = 0{\cdot}25$, ——; (*b*) $\dot{\gamma} = 0{\cdot}5$, □; and (*c*) $\dot{\gamma} = 1{\cdot}0$, △.

The transient responses, P_{XY}, for pure shear applied to the near triple point state are given in figure 4. The viscosities obtained at $\partial v_X/\partial Y = 0{\cdot}25$, $0{\cdot}5$ and $1{\cdot}0$ are $2{\cdot}80$, $2{\cdot}46$ and $2{\cdot}13 \pm 0{\cdot}03$. We used up to 1040×4 distinct NEMD transient responses. The viscosities are statistically indistinguishable from those obtained in an earlier steady state SLLOD NEMD study [17]. The TCF route to the P_{XY} response using (8) and the same number of transients was found to be statistically inferior. An example of the P_{XY} response at a shear rate of $1{\cdot}0$ is given in figure 5. The pressure tensor component, P_{XX}, responses for $\partial v_X/\partial Y = 0{\cdot}25$, $0{\cdot}5$ and $1{\cdot}0$ are given in figure 6. The P_{XX} exhibits a pronounced 'overshoot' at the largest shear rate considered, reflecting the structural changes occurring in the fluid during the creation of non-Newtonian state. Some structural change must be a feature of a decrease in shear viscosity. The overshoot is an indicator that this is taking place on a timescale comparable to that of the shear stress relaxation time. However, an overshoot does not necessarily accompany shear thinning, as is evident in the P_{XX} responses from the two lower shear rates considered in figure 6.

3.2. *Elongational flow*

We now consider the transient elongational strains applied to the near triple point state. The phase space mappings were chosen to zero the sum of the normal pressure components at $t = 0$ using the combination of normal pressures from (26),

$$\Gamma_2 = (-y, -x, z, -p_x, -p_y, p_z),$$

$$\Gamma_3 = (-z, -x, -y, -p_z, -p_x, -p_y),$$

Other permutations will also achieve this objective.

Making use of two phase space mappings we employed typically 800×3 unique starting points in phase space with a profile unassumed thermostat. We considered

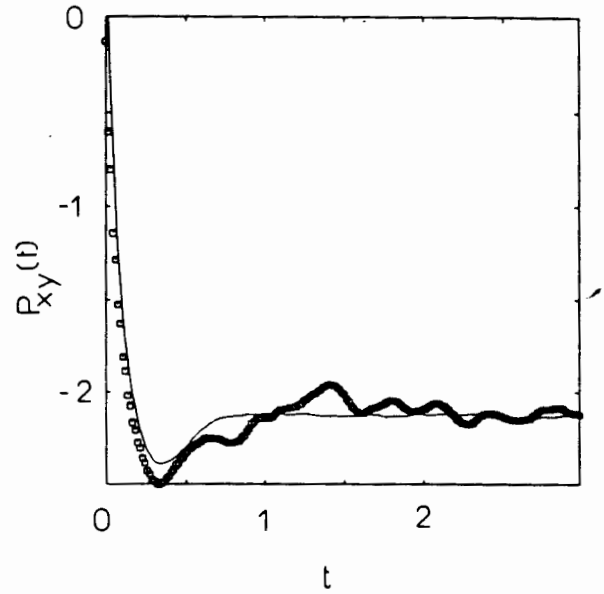

Figure 5. The stress responses, $P_{xy}(t)$, of $\rho = 0{\cdot}8442$ and $T = 0{\cdot}722$, $N = 256$ liquids subjected to a shear strain rate applied at time $t = 0$, $\dot{\gamma} = 1{\cdot}0$, ——, direct response and the transient time correlation function route of (6), □.

a selection of $\dot{\gamma}_T$ with $\delta_X = 1$, $\delta_Y = -1/2$ and $\delta_Z = -1/2$. The expansion of the MD cell in the X direction leads to a decrease in P_{xx}. The contraction in the dimensions of the MD cell in the Y and Z directions creates an increase in P_{yy}. (The equilibrium pressure at this $N = 256$ state point is $0{\cdot}100 \pm 0{\cdot}004$. The equilibrium total

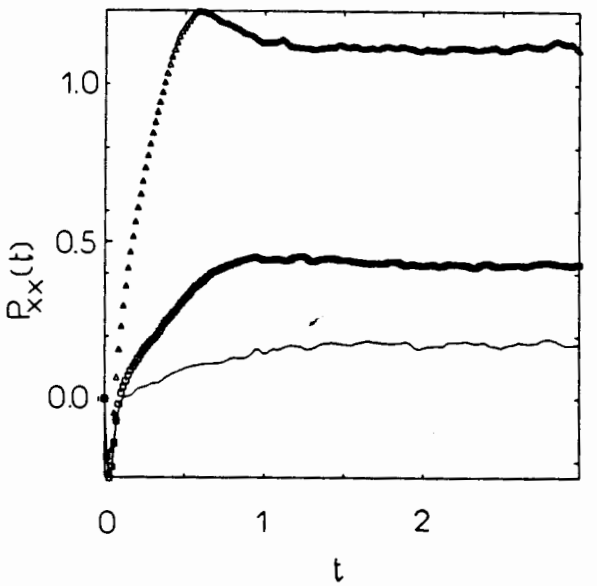

Figure 6. The normal pressure response, $P_{xx}(t)$, of $\rho = 0{\cdot}8442$ and $T = 0{\cdot}722$, $N = 256$ liquids subjected to shear strain rates applied at time $t = 0$: (*a*) $\dot{\gamma} = 0{\cdot}25$, ——; (*b*) $\dot{\gamma} = 0{\cdot}5$, □; and (*c*) $\dot{\gamma} = 1{\cdot}0$, △.

$P_{xx}(t)$

Figure 7. Elongation: normal pressure liquids subjected P_{yy}, □; and (*c*)

internal energy per p ment of the change ir using table 2 that, ir than the increase in fluids to extension wl

We prefer to use $\dot{\gamma}_T \to 0$ limit then the Trouton's rile in the ous link between η a of different symmet [17].) Figure 8 prese and 0·098. The deriv 0·197, respectively. regime, equivalent t cosities fit reasonab energy ('temperatur is a noticeable chan the total energy per

We now consid strain rates. Both al not able to devise and elongational sy the elongational flo

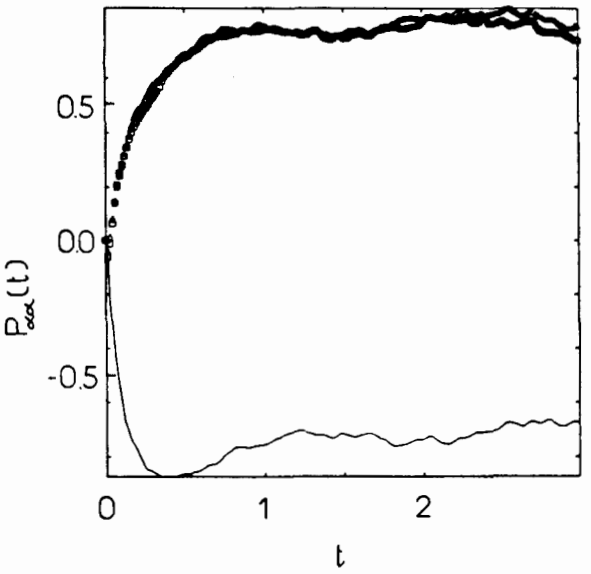

Figure 7. Elongational flow with $\delta_X = 1$, $\delta_Y = -1/2$ and $\delta_Z = -1/2$. $\partial v_x/\partial y = 0$. The normal pressure responses, $P_{\alpha\alpha}(t)$, of $\rho = 0{\cdot}8442$, $T = 0{\cdot}722$, $\dot{\gamma}_T = 0{\cdot}197$ and $N = 256$ liquids subjected to elongational strain rates applied at time $t = 0$: (*a*) P_{XX}, ——; (*b*) P_{YY}, □; and (*c*) P_{ZZ}, △.

internal energy per particle is $-5{\cdot}020 \pm 0{\cdot}001$.) Figure 7 shows the time development of the change in $P_{\alpha\alpha}$ as a result of the elongational strain, $\dot{\gamma}_T = 0{\cdot}197$. We note using table 2 that, in this non-newtonian regime the decrease in P_{XX} becomes less than the increase in P_{YY} or P_{ZZ} with increasing $\dot{\gamma}_T$. This reflects the weakness of fluids to extension when compared to compression.

We prefer to use $\eta_T/3$ when discussing the elongational viscosity because in the $\dot{\gamma}_T \to 0$ limit then the Navier–Stokes equation gives $\eta = \eta_T/3$ [9]. This is known as Trouton's rile in the rheological community. At finite strain rates there is no rigorous link between η and η_T because the two types of strain cause structural changes of different symmetries. (The newtonian viscosity at this state point is $3{\cdot}5 \pm 0{\cdot}1$ [17].) Figure 8 presents the derived $P_{XX} - P_{YY}/2 - P_{ZZ}/2$ and those from $\dot{\gamma}_T = 0{\cdot}049$ and $0{\cdot}098$. The derived $\eta_T/3$ are $3{\cdot}37$, $2{\cdot}88$ and $2{\cdot}70 \pm 0{\cdot}03$ for $\dot{\gamma}_T = 0{\cdot}049$, $0{\cdot}098$ and $0{\cdot}197$, respectively. We therefore are within an elongational viscosity thinning regime, equivalent to a shear rate $\leqslant 0{\cdot}25$ for shear thinning. The elongational viscosities fit reasonably well to a $\dot{\gamma}_T^{1/2}$ power law. Although the volume and kinetic energy ('temperature') of the MD cell does not change during the elongation, there is a noticeable change in the 'thermodynamic' state of the system. This is evident in the total energy per particle responses for the above three $\dot{\gamma}_T$, plotted in figure 9.

3.3. *Elongational and shear flow*

We now consider the effects of *simultaneously applied* shear and elongational strain rates. Both algorithms present no problems when used concurrently. We were not able to devise phase space mappings that would simultaneously satisfy shear and elongational symmetries. In response, we used the same (two) mappings as for the elongational flow. The details of the results of these simulations are summarised

Table 2. Plateau averages taken from the transient response simulations of shear and elongational flow. The symbols are defined in the text. ON is the number of equilibrium segments. The property averages are taken from plateau regions before material degradation ultimately dominated.

$\dot{\gamma}$	δ_x	δ_y	δ_z	$\dot{\gamma}_T$	ON	η	$\eta_T/3$	P_{xx}	P_{yy}	P_{zz}	P_{xy}	E	N
0·25	—	—	—	0·0	560	2·80	—	0·17	0·22	0·18	−0·70	0·038	256
0·5	—	—	—	0·0	1040	2·46	—	0·43	0·50	0·37	−1·23	0·087	256
1·0	—	—	—	0·0	940	2·13	—	1·11	1·24	0·82	−2·11	0·22	256
0·0	1	−1/2	−1/2	0·030	360	0	3·44	−0·18	0·11	0·14	0·0	0·004	256
0·0	1	−1/2	−1/2	0·049	720	0	3·37	−0·27	0·21	0·22	0·0	0·011	256
0·0	1	−1/2	−1/2	0·059	360	0	3·28	−0·31	0·26	0·26	0·0	0·013	256
0·0	1	−1/2	−1/2	0·098	726	0	2·88	−0·49	0·37	0·36	0·0	0·013	256
0·0	1	−1/2	−1/2	0·197	362	0	2·70	−0·67	0·78	0·79	0·0	0·048	256
0·05	1	−1/2	−1/2	0·0689	320	2·2	2·95	−0·32	0·27	0·27	−0·11	0·015	256
0·05	1	−1/2	−1/2	0·0246	240	2·2	3·5	−0·14	0·11	0·13	−0·11	0·010	256
0·05	1	−1/2	−1/2	0·0492	400	2·2	3·3	−0·27	0·20	0·22	−0·11	0·010	256
0·05	1	−1/2	−1/2	0·0689	320	2·2	3·1	−0·35	0·29	0·29	−0·1	0·017	256
0·05	1	−1/2	−1/2	0·0985	160	2·0	2·9	−0·45	0·42	0·43	−0·10	0·025	256
0·1	1	−1/2	−1/2	0·0246	640	2·5	3·47	−0·13	0·11	0·12	−0·25	0·009	256
0·1	1	−1/2	−1/2	0·0864	120	2·2	2·85	−0·45	0·28	0·29	−0·22	0·012	500
0·1	1	−1/2	−1/2	0·173	120	3·1	2·7	−0·75	0·63	0·64	−0·31	0·034	500
0·25	1	−1/2	−1/2	0·0246	560	2·5	3·31	0·04	0·29	0·29	−0·63	0·042	256
0·25	1	−1/2	−1/2	0·049	640	2·2	2·93	−0·12	0·30	0·30	−0·54	0·028	256
0·25	1	−1/2	−1/2	0·0605	90	2·6	2·98	−0·21	0·34	0·32	−0·65	0·033	500
0·25	1	−1/2	−1/2	0·0689	720	2·4	2·9	−0·22	0·40	0·40	−0·59	0·038	256
0·25	1	−1/2	−1/2	0·121	210	2·2	2·73	−0·48	0·53	0·50	−0·55	0·037	500
0·25	1	−1/2	−1/2	0·121	150	2·2	2·7	−0·43	0·56	0·50	−0·55	0·044	500
0·25	1	−1/2	−1/2	0·172	60	(1·96)	2·5	(−0·57)	(0·71)	(0·70)	−0·49	0·051	500
0·5	1	−1/2	−1/2	0·0492	240	2·2	2·6	0·16	0·60	0·48	−1·1	0·083	256
0·5	1	−1/2	−1/2	0·0985	240	2·0	2·4	−0·08	0·67	0·58	−1·0	0·080	256
0·75	1	−1/2	−1/2	0·0985	240	2·1	2·4	0·27	1·09	0·77	−1·6	0·11	256
0·05	−1/2	1	−1/2	0·148	160	3·2	2·6	0·58	−0·57	0·61	−0·16	0·040	256
0·1	−1/2	1	−1/2	0·0492	320	3·3	3·05	0·26	−0·20	0·24	−0·33	0·012	256
0·1	−1/2	1	−1/2	0·1477	400	3·4	2·3	0·54	−0·47	0·53	−0·34	0·039	256
0·25	−1/2	1	−1/2	0·0246	240	2·96	2·8	0·29	0·07	0·27	−0·74	0·041	256
0·25	−1/2	1	−1/2	0·049	720	2·92	2·72	0·59	0·28	0·57	−0·80	0·097	256
0·25	−1/2	1	−1/2	0·049	400	2·92	2·72	0·34	−0·05	0·34	−0·73	0·044	256
0·25	−1/2	1	−1/2	0·1477	240	2·96	2·5	0·72	−0·40	0·71	−0·74	0·067	256

Figure 8. Elongationa
normal pressure
$N = 256$ liquids
0·049, ——; (*b*) $\dot{\gamma}$

in table 2. These con
many cross-effects, hi
First, we will con
strain distortions ar

$P_{xx} - P_{yy}/2 - P_{zz}/2$

Figure 9. Elongatio
energy per pa
subjected to el
$\dot{\gamma}_T = 0{\cdot}098$, □

E

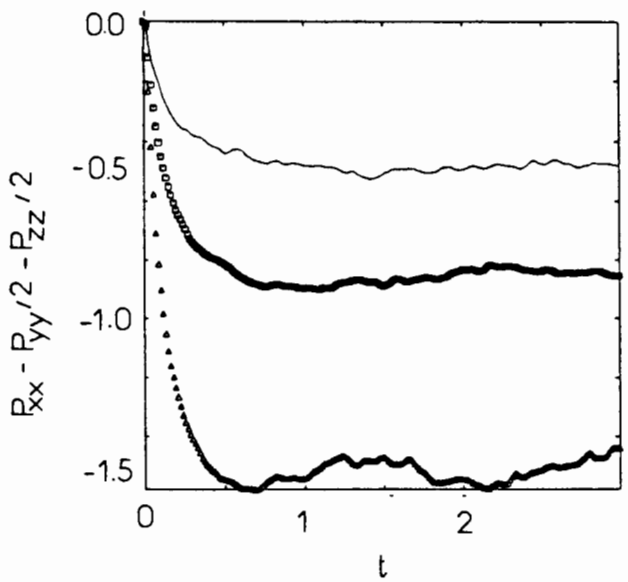

Figure 8. Elongational flow with $\delta_X = 1$, $\delta_Y = -1/2$ and $\delta_Z = -1/2$. $\partial v_X/\partial y = 0$. The normal pressure responses, $P_{XX}(t) - P_{YY}(t)/2 - P_{ZZ}(t)/2$, of $\rho = 0{\cdot}8442$, $T = 0{\cdot}722$, and $N = 256$ liquids subjected to elongational strain rates applied at time $t = 0$: (*a*) $\dot{\gamma}_T = 0{\cdot}049$, ——; (*b*) $\dot{\gamma}_T = 0{\cdot}098$, □; and (*c*) $\dot{\gamma}_T = 0{\cdot}197$, Δ.

in table 2. These combined flows, which are to a certain extent conflicting, produce many cross-effects, highlighted in the discussion below.

First, we will consider extension in the streaming direction of the shear flow. The strain distortions are defined by $\dot{\gamma}$ $(= \partial v_X/\partial Y)$ and $\delta_X = 1$, $\delta_Y = -1/2$ and $\delta_Z =$

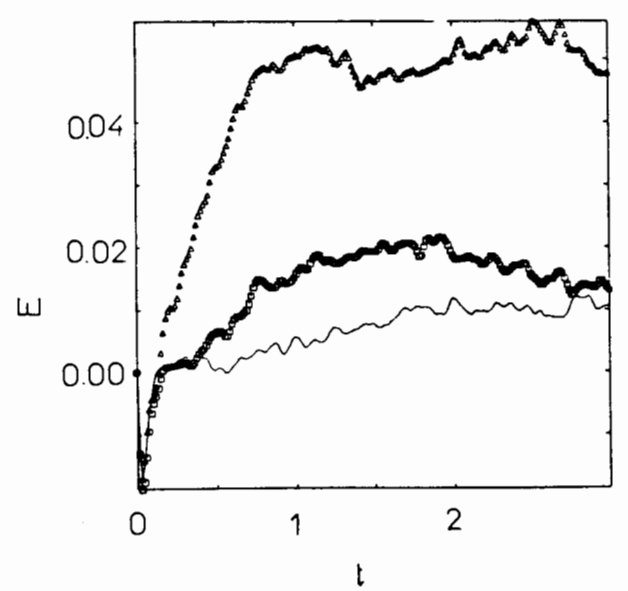

Figure 9. Elongational flow with $\delta_X = 1$, $\delta_Y = -1/2$ and $\delta_Z = -1/2$. $\partial v_x/\partial y = 0$. The total energy per particle responses, $E(t)$, of $\rho = 0{\cdot}8442$, $T = 0{\cdot}722$, and $N = 256$ liquids subjected to elongational strain rates applied at time $t = 0$: (*a*) $\dot{\gamma}_T = 0{\cdot}049$, ——; (*b*) $\dot{\gamma}_T = 0{\cdot}098$, □; and (*c*) $\dot{\gamma}_T = 0{\cdot}197$, Δ.

$-1/2$. In figure 10 the $P_{xy}(t)$ for a selection of $\dot{\gamma}_T$ are given. In the figure $t = 0$ coincides with the commencement of application of the two types of strain rates. At ($\dot{\gamma} = 0{\cdot}1$, $\dot{\gamma}_T = 0{\cdot}0246$), we have a $t \to \infty$ asymptotic P_{xy} that yields $\eta = 2{\cdot}50 \pm 0{\cdot}05$, which is significantly lower than the shear viscosity at this shear rate in the absence of elongational flow ($= 3{\cdot}0 \pm 0{\cdot}1$ [17]). Similarly at ($\dot{\gamma} = 0{\cdot}25$, $\dot{\gamma}_T = 0{\cdot}0492$), we have $\eta = 2{\cdot}20 \pm 0{\cdot}05$, which compares with $\eta = 2{\cdot}76 \pm 0{\cdot}03$ in the absence of elongational flow. We ascribe this enhanced shear thinning to the action of the elongational flow in 'dynamically ordering' the fluid along the stream lines of the shear flow (X direction). The elongational flow facilitates the mechanism that causes shear thinning in simple fluids. At $\dot{\gamma} = 1{\cdot}0$ and $\dot{\gamma}_T = 0{\cdot}197$ we observe no plateau in $P_{xy}(t \to \infty)$ but a steady decline in magnitude beyond an initial ascent at short time ($t < 0{\cdot}4$). Under these circumstances it is not meaningful to characterize this flow in terms of a 'viscosity' as there is no plateau in either the shear or elongational stress. The response is purely viscoelastic. The plateaus in the shear and elongational stresses coincide in time. Beyond the plateaus most of the simulations manifested a decrease in the shear and elongational stresses, reflecting, unbounded structural degradation.

Figure 11 reveals that there is a similar pattern in η_T on the application of a simultaneous elongation and shear of the same relative orientation. The induced elongational viscosities are listed in table 2. We note that the elongational viscosity at fixed $\dot{\gamma}_T$, decreases when accompanied by shear flow.

In the limit of small shear rate ($\dot{\gamma} \sim 0{\cdot}05$) and elongation rate, ($\dot{\gamma}_T \leqslant 0{\cdot}1$), table 2 reveals that there is the greatest elongation enhancement in shear thinning ($\eta(\dot{\gamma}) \leqslant (0)$). It would appear that for larger $\dot{\gamma}_T \sim 0{\cdot}2$ and $\dot{\gamma} \sim 0{\cdot}25$ the two flows combined do not produce such a dramatic relative decrease in each of the viscosities.

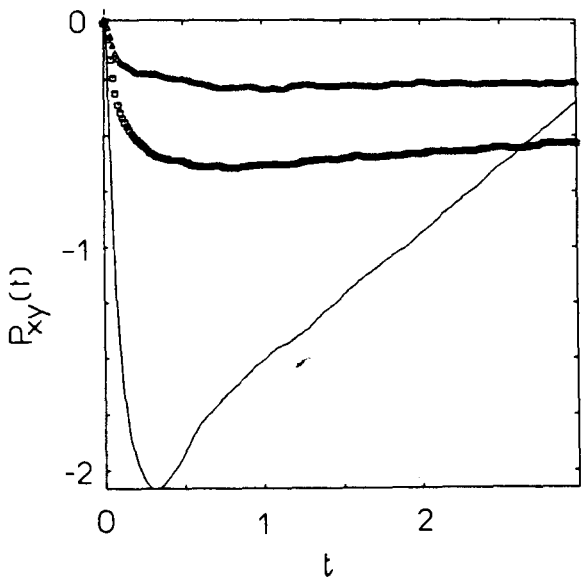

Figure 10. A combination of shear flow, $\dot{\gamma} = \partial v_X/\partial Y$, and elongational flow with $\delta_X = 1$, $\delta_Y = -1/2$ and $\delta_Z = -1/2$. The P_{XY} responses of $\rho = 0{\cdot}8442$, $T = 0{\cdot}722$, and $N = 256$ liquids: (a) $\dot{\gamma} = 1{\cdot}0$, $\dot{\gamma}_T = 0{\cdot}197$, ——, (*b*) $\dot{\gamma} = 0{\cdot}25$, $\dot{\gamma}_T = 0{\cdot}049$, □; and (*c*) $\dot{\gamma} = 0{\cdot}1$, $\dot{\gamma}_T = 0{\cdot}0246$, △.

$P_{xx} - P_{yy}/2 - P_{zz}/2$

Figure 11. A combin
$\delta_Y = -1/2$ and
$T = 0{\cdot}722$, and
□; and (*c*) $\dot{\gamma} =$ (

Computations w
tive alignment of th
and $\delta_Z = -1/2$. Thi
to the streaming (x)
and elongational flo
bined flow in order
flow into a contrac
other) classes at diff

Table 2 reveals
effect of the shear
accompanied by a
extent of shear thin
at $\dot{\gamma} = 0{\cdot}25$ and $\dot{\gamma}_T$
have $\eta = 2{\cdot}76$ [17].
flow is to compress
rides expansion in
presence of 'orthog
facilitated when th
evident for the per
elongation in the z
future study. The
interest.

In figures 12(*a*)
shear rate and vari
note that at this $\dot{\gamma}$

ven. In the figure $t = 0$
types of strain rates. At
t yields $\eta = 2{\cdot}50 \pm 0{\cdot}05$,
hear rate in the absence
5, $\dot{\gamma}_T = 0{\cdot}0492$), we have
1 the absence of elon-
the action of the elon-
tream lines of the shear
anism that causes shear
observe no plateau in
tial ascent at short time
characterize this flow in
r or elongational stress.
shear and elongational
mulations manifested a
unbounded structural

on the application of a
ientation. The induced
e elongational viscosity

rate, ($\dot{\gamma}_T \leqslant 0{\cdot}1$), table 2
nt in shear thinning
$\sim 0{\cdot}25$ the two flows
se in each of the vis-

ional flow with $\delta_X = 1$,
$T = 0{\cdot}722$, and $N = 256$
19, □; and (*c*) $\dot{\gamma} = 0{\cdot}1$,

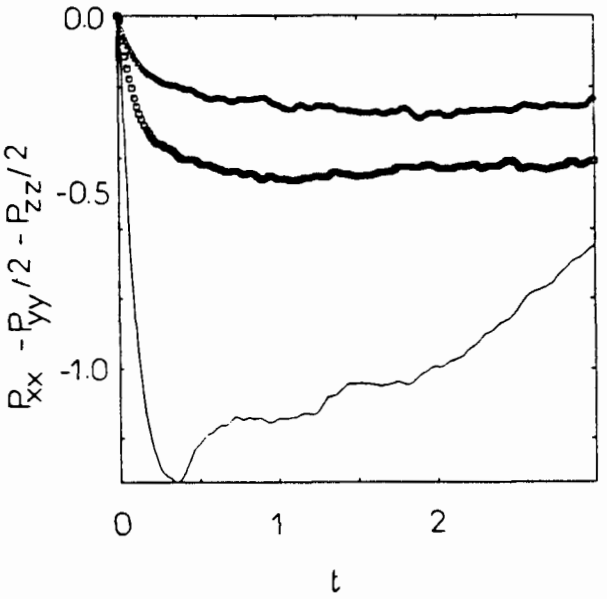

Figure 11. A combination of shear flow, $\dot{\gamma} = \partial v_X/\partial Y$, and elongational flow with $\delta_X = 1$, $\delta_Y = -1/2$ and $\delta_Z = -1/2$. The $P_{XX} - P_{YY}/2 - P_{ZZ}/2$ time responses of $\rho = 0{\cdot}8442$, $T = 0{\cdot}722$, and $N = 256$ liquids: (*a*) $\dot{\gamma} = 1{\cdot}0$, $\dot{\gamma}_T = 0{\cdot}197$, ——; (*b*) $\dot{\gamma} = 0{\cdot}25$, $\dot{\gamma}_T = 0{\cdot}049$, □; and (*c*) $\dot{\gamma} = 0{\cdot}1$, $\dot{\gamma}_T = 0{\cdot}0246$, △.

Computations were also carried out with an orthogonal or perpendicular relative alignment of the two fluids, specified by: $\dot{\gamma}$ ($= \partial v_X/\partial Y$) and $\delta_X = -1/2$, $\delta_Y = 1$ and $\delta_Z = -1/2$. This flow has the extension of the fluid taking place perpendicular to the streaming (x) direction. This gives rise to the class of 'perpendicular' shear and elongational flow combinations. We have considered these two classes of combined flow in order to clarify the general trends. In any practical arrangement (e.g. flow into a contraction), the flow will be a linear combination of these two (and other) classes at different points in the flow field.

Table 2 reveals that this perpendicular flow combination has a quite different effect of the shear viscosity. There is still $\dot{\gamma}$ induced shear thinning in η, when accompanied by a finite $\dot{\gamma}_T$. However, the elongational flow acts to diminish the extent of shear thinning when compared with the unelongated sample. For example, at $\dot{\gamma} = 0{\cdot}25$ and $\dot{\gamma}_T = 0{\cdot}049$ $\eta = 2{\cdot}92$, whereas at the same shear rate but $\dot{\gamma}_T = 0$ we have $\eta = 2{\cdot}76$ [17]. (Note $\eta = 3{\cdot}5$ for $\dot{\gamma} \to 0$.) The effect of this class of elongational flow is to compress the particles in the streaming direction. This we suggest, overrides expansion in the y direction, leading to less shear thinning at finite $\dot{\gamma}$ in the presence of 'orthogonal' $\dot{\gamma}_T$. We conclude that flow in the non-newtonian regime is facilitated when the major streaming directions are parallel. The opposite trend is evident for the perpendicular arrangement. The remaining flow arrangements (with elongation in the z direction) and 'compressional' flows remain to be treated in a future study. The state point dependence of these flow arrangements is also of interest.

In figures 12 (*a*), and (*b*) we present the elongational and shear stresses for a fixed shear rate and variable elongation rates with $\delta_X = 1$, $\delta_Y = -1/2$ and $\delta_Z = -1/2$. We note that at this $\dot{\gamma} = 0{\cdot}25$ there is a plateau in the elongational stress but not shear

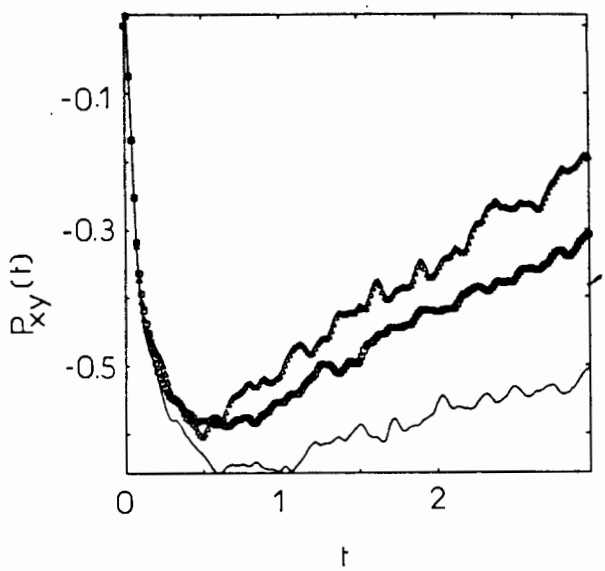

(*a*)

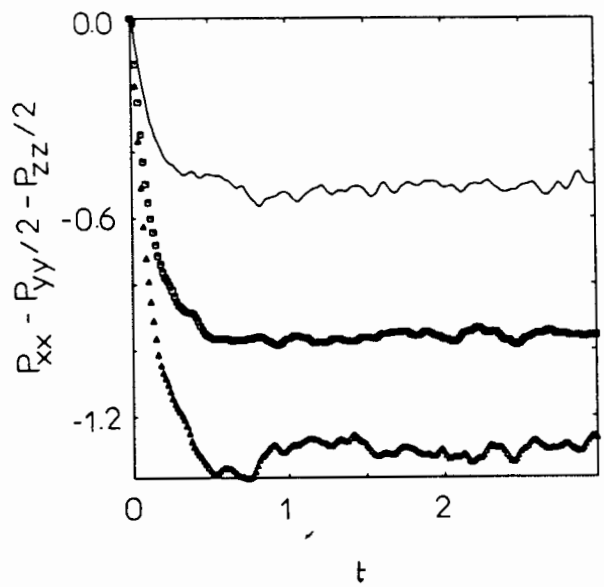

(*b*)

Figure 12. A combination of shear flow, $\dot{\gamma} = \partial v_X/\partial Y$, and elongational flow with $\delta_X = 1$, $\delta_Y = -1/2$ and $\delta_Z = -1/2$. The pressure tensor responses for $\rho = 0{\cdot}8442$, $T = 0{\cdot}722$, $\dot{\gamma} = 0{\cdot}25$ and $N = 500$ liquids. (*a*) $P_{XY}(t)$, $\dot{\gamma}_T = 0{\cdot}0605$, ——; $\dot{\gamma}_T = 0{\cdot}121$, □; and $\dot{\gamma}_T = 0{\cdot}173$, △. (*b*) as for (*a*), except $P_{XX} - P_{YY}/2 - P_{ZZ}/2$ are given.

Figure 13. A combi
$\delta_Y = 1$ and δ
$\dot{\gamma} = 0{\cdot}25$ and
$\dot{\gamma}_T = 0{\cdot}1472$, ι

stress; the elongational flow field dominates. In figures 13(*a*),(*b*) we present the elongational and shear stresses for a fixed shear rate and variable elongation rates with $\delta_X = -1/2$, $\delta_Y = 1$ and $\delta_Z = -1/2$. We again note that at this $\dot{\gamma} = 0{\cdot}25$ there is a plateau in the elongational stress but not in the shear stress. In the limit of both

ational flow with $\delta_X = 1$,
or $\rho = 0{\cdot}8442$, $T = 0{\cdot}722$,
$\dot{\gamma}_T = 0{\cdot}121$, □; and $\dot{\gamma}_T =$

(*a*),(*b*) we present the
riable elongation rates
it this $\dot{\gamma} = 0{\cdot}25$ there is
s. In the limit of both

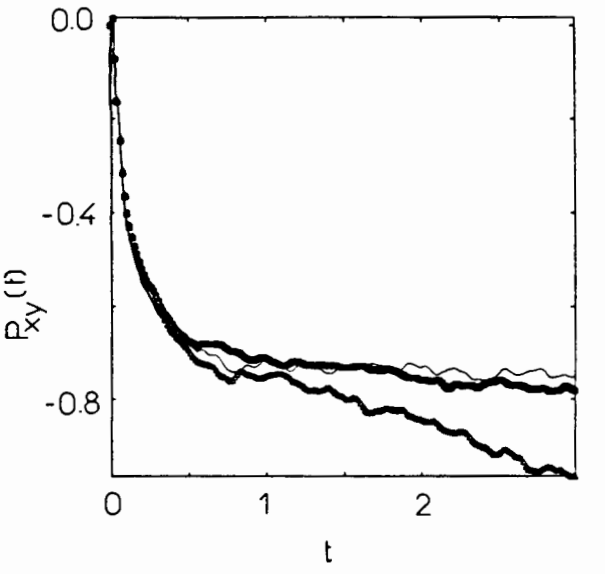

(*a*)

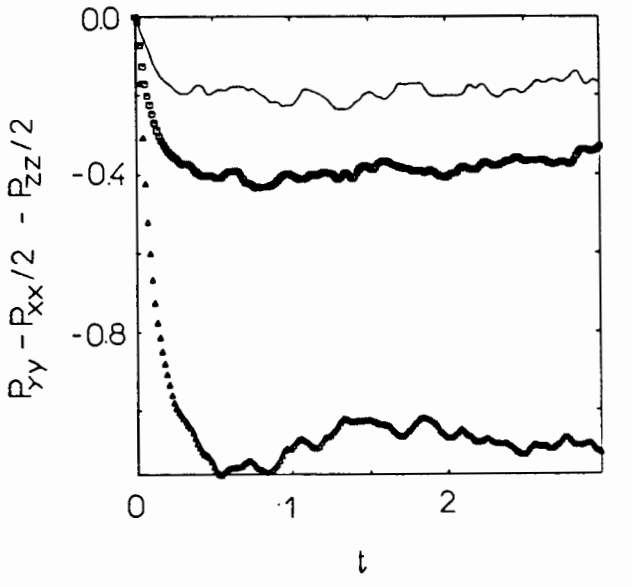

(*b*)

Figure 13. A combination of shear flow, $\dot{\gamma} = \partial v_X/\partial Y$, and elongational flow with $\delta_X = -1/2$, $\delta_Y = 1$ and $\delta_Z = -1/2$. The pressure tensor responses for $\rho = 0{\cdot}8442$, $T = 0{\cdot}722$, $\dot{\gamma} = 0{\cdot}25$ and $N = 256$ liquids. (*a*) $P_{XY}(t)$, $\dot{\gamma}_T = 0{\cdot}0246$, ——; $\dot{\gamma}_T = 0{\cdot}0492$, □; and $\dot{\gamma}_T = 0{\cdot}1472$, △. (*b*) as for (*a*), except $P_{YY} - P_{XX}/2 - P_{ZZ}/2$ are given.

large $\dot{\gamma}$ and $\dot{\gamma}_T$ we find that the behaviour of the $P_{\alpha\alpha}$ and P_{XY} are closely linked. The tendency of the $\dot{\gamma}_T$ is to split the values of $P_{\alpha\alpha}$ in sign according to the signs of δ_α (e.g. in figure 14). The shear flow, in contrast, promotes all diagonal pressure tensor components to become positive (e.g. see figure 15). The outcome in any simulation depends on the relative magnitudes of $\dot{\gamma}$ and $\dot{\gamma}_T$ and the competition between the somewhat conflicting preferences of the two flows.

Combined shear and elongational flow also produce an anomalous thermal effect with induced heat flux. The Green–Kubo integral of the tensor correlation function, $\langle J(t)J(0)\rangle$ provides scalar elements of the thermal conductivity [22]. The two flows in the orthogonal configuration produce a heat flux analogous to the Weissenberg effect for the diagonal components of the pressure tensor (e.g. figure 16). Pure shear, pure elongation and the shear/elongation arrangement, $\dot{\gamma}\,(=\partial v_X/\partial Y)$ and $\delta_X = 1$, $\delta_Y = -1/2$ and $\delta_Z = -1/2$, do not produce any noticeable heat flux. The full D symmetry of shear and elongation together is $D_u^{(1)} D_u^{(1)} = D_s^{(0)} + D_s^{(1)} + D_s^{(2)}$. This accounts for the simultaneous presence of both diagonal and off-diagonal elements. The full D symmetry of thermal conductivity is that of the integral over the correlation function of the Irving/Kirkwood heat flux tensor J, i.e. $(D_u^{(1)} D_u^{(1)})$. Therefore the full D symmetry of thermal conductivity includes the full D symmetry of combined elongational and shear flow, consistent with principle (3) of GTSM. Symmetry indicates whether a process can occur but not that it will occur. Therefore the failure of pure shear or elongation to create this heat flux is a demonstration of this fact.

The transient correlation functions for the elongation fluids manifest the symmetry splitting predicted by (10). In the absence of elongation or shear, $\langle P_{XX}(0)P_{XX}(t)\rangle = \langle P_{YY}(0)P_{YY}(t)\rangle = \langle P_{ZZ}(0)P_{ZZ}(t)\rangle$. In contrast, with elongation

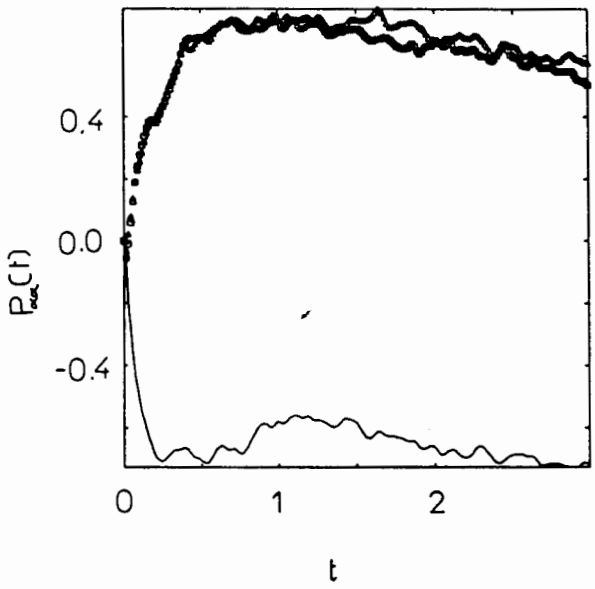

Figure 14. A combination of shear flow, $\dot{\gamma} = \partial v_X/\partial Y$, and elongational flow with $\delta_X = 1$, $\delta_Y = -1/2$ and $\delta_Z = -1/2$. The $P_{\alpha\alpha}$ time responses of $\rho = 0{\cdot}8442$, $T = 0{\cdot}722$, and $N = 500$ liquids with $\dot{\gamma} = 0{\cdot}25$ and $\dot{\gamma}_T = 0{\cdot}173$: (*a*) P_{XX}, ——; (*b*) P_{YY}, □; and (*c*) P_{ZZ}, △.

$P_{xx}(t)$

Figure 15. A combin
$\delta_Y = 1$ and $\delta_Z =$
liquids with $\dot{\gamma} =$

these component c
parallel and perpen
17 (*a*),(*b*) respectivel
argument, $t = 0$, is

Figure 16. A combi
$\delta_Y = 1$ and δ_Z
and $N = 256$
△.

$_{XY}$ are closely linked. The
ling to the signs of δ_α (e.g.
diagonal pressure tensor
ıtcome in any simulation
competition between the

: an anomalous thermal
of the tensor correlation
ıl conductivity [22]. The
ıt flux analogous to the
essure tensor (e.g. figure
rrangement, $\dot{\gamma}$ $(=\partial v_X/\partial Y)$
ıny noticeable heat flux.
is $D_u^{(1)} D_u^{(1)} = D_g^{(0)} + D_g^{(1)}$
both diagonal and off-
ductivity is that of the
ɔd heat flux tensor J, i.e.
tivity includes the full D
tent with principle (3) of
ut not that it will occur.
his heat flux is a demon-

fluids manifest the sym-
elongation or shear,
trast, with elongation

ıtional flow with $\delta_X = 1$,
= 0·8442, $T = 0·722$, and
; (*b*) P_{YY}, □; and (*c*) P_{ZZ},

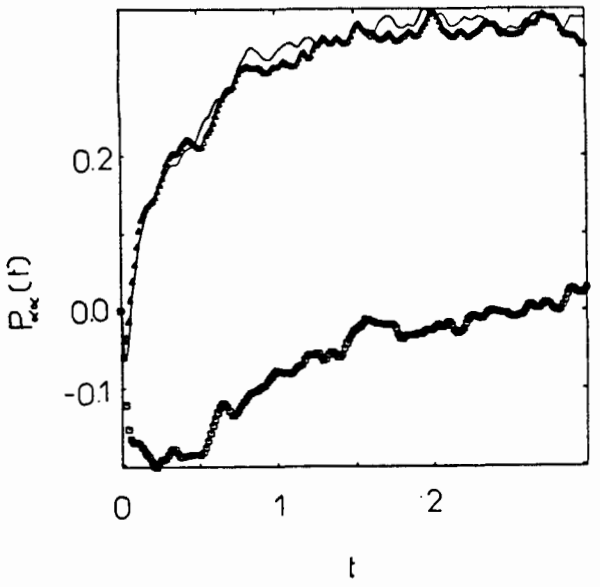

Figure 15. A combination of shear flow, $\dot{\gamma} = \partial v_X/\partial Y$, and elongational flow with $\delta_X = -1/2$, $\delta_Y = 1$ and $\delta_Z = -1/2$. The $P_{\alpha\alpha}$ time responses of $\rho = 0·8442$, $T = 0·722$, and $N = 256$ liquids with $\dot{\gamma} = 0·25$ and $\dot{\gamma}_T = 0·0492$: (*a*) P_{XX}, ——; (*b*) P_{YY}, □; and (*c*) P_{ZZ}, △.

these component correlation functions are split as given in figure 17, shown for parallel and perpendicular arrangements of shear and elongational strain, in figures 17(*a*),(*b*) respectively. (In these time correlation functions the quantity with time argument, $t = 0$, is taken from the equilibrium ensemble, whereas the quantity at

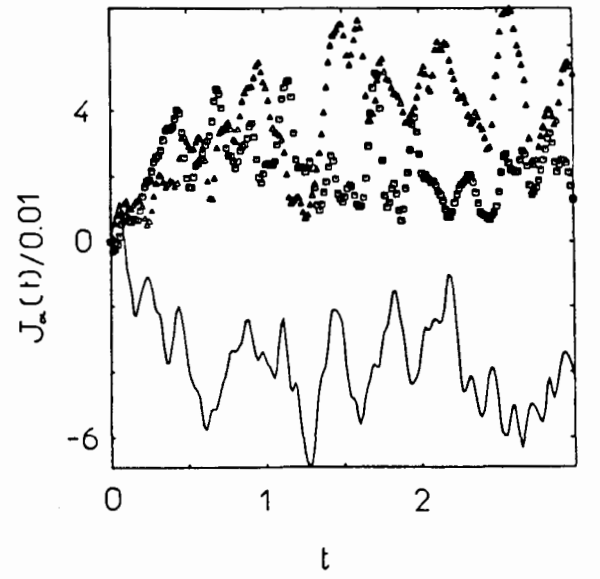

Figure 16. A combination of shear flow, $\dot{\gamma} = \partial v_X/\partial Y$, and elongational flow with $\delta_X = -1/2$, $\delta_Y = 1$ and $\delta_Z = -1/2$. The heat current J_α time responses of $\rho = 0·8442$, $T = 0·722$, and $N = 256$ liquids with $\dot{\gamma} = 0·25$ and $\dot{\gamma}_T = 0·148$: (*a*) J_X, ——; (*b*) J_Y, □; and (*c*) J_Z, △.

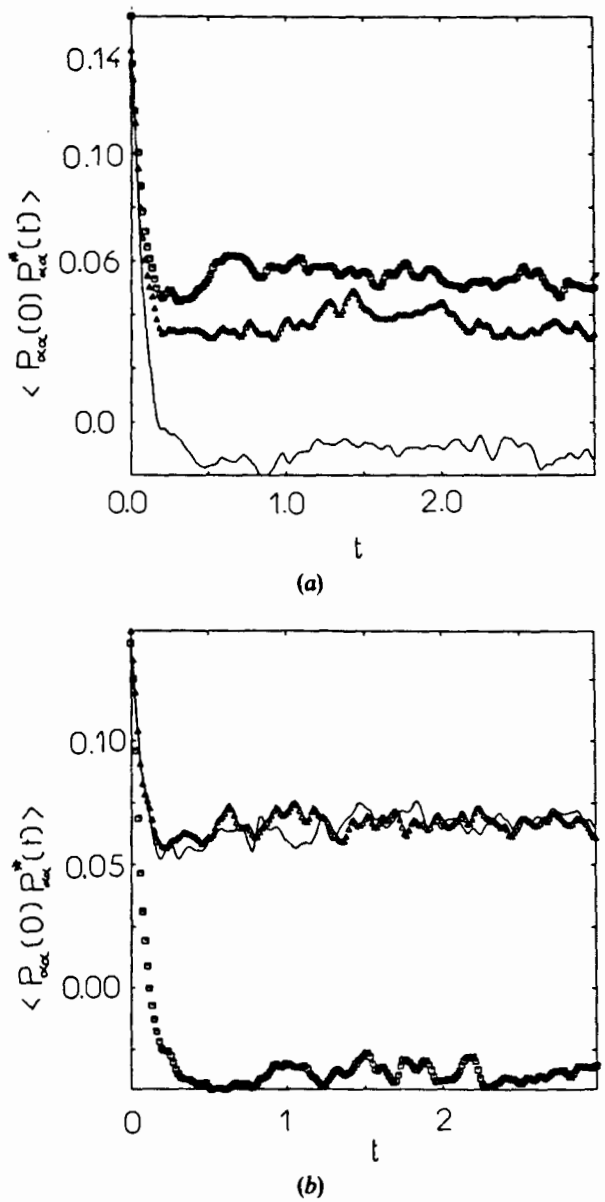

Figure 17. Some transient time correlation functions, $\langle P^*_{\alpha\alpha}(0)P^*_{\alpha\alpha}(t)\rangle$ for LJ states subjected to simultaneous shear and elongational strain rates. The * denotes the perturbed state. (*a*) $\dot{\gamma} = \partial v_X/\partial Y = 0{\cdot}25$, and elongational flow with $\dot{\gamma}_T = 0{\cdot}0689$, $\delta_X = 1$, $\delta_Y = -1/2$ and $\delta_Z = -1/2$, 3×720 segments, $N = 256$. $\alpha = X$, line, $\alpha = Y$, □; and $\alpha = Z$, △. (*b*) $\dot{\gamma} = \partial v_X/\partial Y = 0{\cdot}1$, and elongational flow with $\gamma_T = 0{\cdot}148$, $\delta_X = -1/2$, $\delta_Y = 1$ and $\delta_Z = -1/2$, $N = 256$. $\alpha = X$, line, $\alpha = Y$, □; and $\alpha = Z$, △.

$t > 0$ is taken from the transient ensemble.) If the accompanying shear rate is sufficiently large then the $\langle P_{YY}(0)P_{YY}(t)\rangle \neq \langle P_{ZZ}(0)P_{ZZ}(t)\rangle$ for $\delta_X = 1$, $\delta_Y = -1/2$ and $\delta_Z = -1/2$ elongation. The degeneracy between Y and Z directions from the elongation is broken by the superimposed shear flow. This is evident in figure 17(*a*).

When the elonga
$\langle P_{ZZ}(0)P_{ZZ}(t)\rangle$ in δ_X
17(*b*). In this case th
degeneracy of perper

In this report we
gational flow. We ha
and enable us to ext
symmetries leading
simultaneously appl
non-newtonian visc
tions of the flow fi
symmetry of combin
shortcomings of pre
these many-body ef
ducing the complex
non-newtonian liqui

D.M.H. gratefull
1983 University Res
Honorary Research
at the University of
for use of their VAX

[1] Evans, M. W., a
[2] Evans, M. W., 1
[3] Onsager, L., 19
[4] Onsager, L., 19
[5] Resibois, P., an
Interscience).
[6] Tomita, K., and
[7] Evans, M. W.,
Dynamics (Wil
[8] Evans, M. W., a
[9] Heyes, D. M., 1
[10] Heyes, D. M., 1
[11] Morriss, G. P.,
[12] Morriss, G. P.,
[13] Morriss, G. P.,
[14] Heyes, D. M., 1
[15] Woodcock, L. V
[16] MacGowan, D.
[17] Heyes, D. M., 1
[18] Evans, D. J., an
[19] Evans, D. J., an
[20] Hanley, H. J. M
149, 406.
[21] Heyes, D. M., a
[22] Evans, D. J., 19
[23] Binding, D. M.
A, 323, 449.

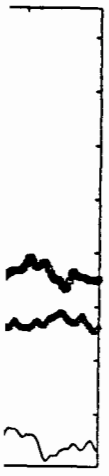

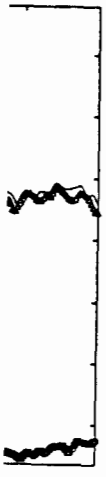

$P_{\alpha\alpha}(t)\rangle$ for LJ states subjected
denotes the perturbed state.
689, $\delta_X = 1$, $\delta_Y = -1/2$ and
$= Y$, □; and $\alpha = Z$, △. (*b*)
48, $\delta_X = -1/2$, $\delta_Y = 1$ and

ompanying shear rate is
$\rangle$ for $\delta_X = 1$, $\delta_Y = -1/2$
nd Z directions from the
is evident in figure 17 (*a*).

When the elongation dominates the shear flow then $\langle P_{XX}(0)P_{XX}(t)\rangle \simeq \langle P_{ZZ}(0)P_{ZZ}(t)\rangle$ in $\delta_X = -1/2$, $\delta_Y = 1$ and $\delta_Z = -1/2$ elongation, as shown in figure 17 (*b*). In this case the shear rate is not sufficiently large to overcome the X and Z degeneracy of perpendicular elongational flow.

4. Conclusions

In this report we applied group theory statistical mechanics to shear and elongational flow. We have devised equations of motion that produce elongational flow and enable us to extract the elongational viscosity. We have characterized the strain symmetries leading to time disymmetric correlation functions. We discovered that simultaneously applied shear and elongational flows produce a variety of coupled non-newtonian viscous and viscoelastic phenomena. Also, within certain orientations of the flow fields there are induced heat currents caused by the reduced symmetry of combined shear and elongational flow. These phenomena highlight the shortcomings of present continuum modelling techniques which fail to incorporate these many-body effects. These considerations will surely be important in reproducing the complex flow-rate dependent stream-lines in converging flows involving non-newtonian liquids [23].

D.M.H. gratefully thanks The Royal Society for the award of a Royal Society 1983 University Research Fellowship. M.W.E. thanks RHBNC for the award of an Honorary Research Fellowship. We thank S.E.R.C. for the award of computer time at the University of London Computer Centre, and the RHBNC Computer Center for use of their VAX 11/780 computer facilities.

References

[1] Evans, M. W., and Heyes, D. M., 1988, *Molec. Phys.*, **65**, 1441.
[2] Evans, M. W., 1989, *Physics Lett.* A, **134**, 409.
[3] Onsager, L., 1931, *Phys. Rev.*, **37**, 405.
[4] Onsager, L., 1931, *Phys. Rev.*, **38**, 2265.
[5] Resibois, P., and De Leener, M., 1977, *Classical Kinetic Theory of Fluids* (Wiley Interscience).
[6] Tomita, K., and Tomita, H., 1974, *Prog. theor. Phys.*, **51**, 1731.
[7] Evans, M. W., Evans, G. J., Coffey, W. T., and Grigolini, P., 1982, *Molecular Dynamics* (Wiley Interscience).
[8] Evans, M. W., and Heyes, D. M., *Phys. Rev.* B (submitted).
[9] Heyes, D. M., 1985, *Chem. Phys.*, **98**, 15.
[10] Heyes, D. M., 1986, *Physics Lett.* A, **115**, 42.
[11] Morriss, G. P., and Evans, D. J., 1987, *Phys. Rev.* A, **35**, 792.
[12] Morriss, G. P., and Evans, D. J., 1988, *Phys. Rev.* A, **38**, 4142.
[13] Morriss, G. P., and Evans, D. J., 1989, *Phys. Rev.* A (in the press).
[14] Heyes, D. M., 1988, *Comput. Phys. Rep.*, **8**, 71.
[15] Woodcock, L. V., 1971, *Chem. Phys. Lett.*, **10**, 257.
[16] MacGowan, D., and Heyes, D. M., 1988, *Molec. Simul.*, **1**, 277.
[17] Heyes, D. M., 1986, *J. chem. Soc. Faraday Trans. II*, **82**, 1365.
[18] Evans, D. J., and Morriss, G. P., 1984, *Phys. Rev.* A, **30**, 1528.
[19] Evans, D. J., and Morriss, G. P., 1986, *Phys. Rev. Lett.*, **56**, 2172.
[20] Hanley, H. J. M., Morriss, G. P., Welberry, T. R., and Evans, D. J., 1988, *Physica* A, **149**, 406.
[21] Heyes, D. M., and Szczepanski, R., 1987, *J. chem. Soc. Faraday Trans. II*, **83**, 319.
[22] Evans, D. J., 1982, *Physics Lett.* A, **91**, 457.
[23] Binding, D. M., Walters, K., Dheur, J., and Crochet, M. J., 1987, *Phil. Trans. R. Soc.* A, **323**, 449.